Monthly Notices
of the
ROYAL ASTRONOMICAL SOCIETY

Mon. Not. R. Astron. Soc. **400,** 903–916 (2009) doi:10.1111/j.1365-2966.2009.15498.x

Numerical aspects of low Mach number flows in astrophysics: preconditioning techniques

A. A. Hujeirat[1,2]★ and F.-K. Thielemann[1,2]

[1]*ZAH, Landessternwarte Universität Heidelberg, 69117 Heidelberg, Germany*
[2]*Departement Physik, Universität Basel, CH-4056 Basel, Switzerland*

Accepted 2009 August 5. Received 2009 July 28; in original form 2009 April 23

ABSTRACT

Internal flows inside gravitationally stable astrophysical objects, such as the Sun, normal and compact stars, are rotating, highly compressed and extremely subsonic. Such low Mach number flows are usually encountered when studying, for example, the dynamo action in stars and planets or the nuclear burst on neutron stars and white dwarfs. Handling of such flows numerically on time-scales longer than the dynamical one is complicated and challenging.

The aim of this paper is to address the numerical problems associated with the modelling of internal quasi-stationary, rotating low Mach number flows in stars and to discuss possible solution scenarios.

It is shown that the quasi-symmetric approximate factorization method (AFM) as a pre-conditioner within a non-linear Newton-type defect-correction solution procedure is best suited for modelling quasi-stationary weakly compressible flows with moderate low Mach numbers. This method is robust as it can be applied to model time-dependent compressible flows without further modifications. The AFM-pre-conditioning techniques are shown to be extendable into three dimensions with an arbitrary equation of state. Classical dimensional splitting techniques, however, such as the alternating direction implicit or line-Gauss–Seidel methods are not suited for modelling compressible low Mach number flows.

It is also argued that hot and low Mach number astrophysical flows cannot be considered as an asymptotic limit of incompressible flows, but rather as highly compressed flows with extremely stiff pressure terms. We show that, unlike the pseudo-pressure in incompressible fluids, a Poisson-like treatment for the pressure would smooth unnecessarily physically induced acoustic perturbations, thereby violating the conservation of the total energy.

Results of several hydrodynamical calculations are presented, which demonstrate the capability of the solver to search for solutions, that correspond to stationary, viscous and rotating flows with a Mach number as small as $\mathcal{M} \approx 10^{-3}$ as well as to fluid flows that are subject to ultra-strong Newtonian and general relativistic gravitational fields.

Key words: circumstellar matter – infrared: stars.

1 INTRODUCTION

Among different energy contents, the gravitational and thermal energies in bound astrophysical systems are dominant. The virial theorem states that in the absence of external pressure and surface tension, the total energy of gravitationally bound systems is negative, i.e.

$$-\alpha_1 \frac{GM^2}{R} + 2\left[\mathcal{E}_{\rm th} + \mathcal{E}_{\rm kin}\right] + \beta_1 \frac{\Phi^2}{R} < 0, \tag{1}$$

where α_1, β_1 are constants less than 1 and where

$$\begin{cases} \text{Gravitational energy :} & \mathcal{E}_{\rm grav} = \frac{GM^2}{R} \\ \text{Thermal energy :} & \mathcal{E}_{\rm th} = \frac{3}{2}\int_V P \mathrm{d}V \\ \text{Kinetic energy :} & \mathcal{E}_{\rm kin} = \frac{1}{2}\int_V \rho |V_{\rm f}|^2 \mathrm{d}V \\ \text{Magnetic energy :} & \mathcal{E}_{\rm mag} = \frac{\Phi^2}{R}, \end{cases} \tag{2}$$

where G, Φ, M, R, P, $V_{\rm f}$ denote, respectively, the gravitational constant, the magnetic flux, the mass and radius of the object, pressure and fluid velocity, and d V is an infinitesimal volume element.

The final stage in the evolution of such gravitationally stable systems is characterized by the following energy measure:

$$|\mathcal{E}_{\rm grav}| \geq |\mathcal{E}_{\rm th}| \gg |\mathcal{E}_{\rm kin}|, |\mathcal{E}_{\rm mag}|. \tag{3}$$

★E-mail: AHujeirat@lsw.uni-heidelberg.de (AAH); F-K.Thielemann@unibas.ch (FKT)

© 2009 The Authors. Journal compilation © 2009 RAS

In terms of velocities per mass, this relation is equivalent to

$$V_{\rm g}^2 \geq V_{\rm S}^2 \gg V_{\rm f}^2, V_{\rm A}^2, \tag{4}$$

where the velocities correspond to the self-gravitating energy ($V_{\rm g}^2 \doteq \frac{GM^2}{R}$), thermal, fluid and magnetic (Alfvén) velocities.

Therefore, fluid motions in gravitationally stable astrophysical systems are naturally sub-sonic; hence, the Mach number is relatively low.

For example, helioseismology measurements have revealed that the Sun oscillates on various frequencies. In particular, it has been found that the origin of the 5 min oscillations is a self-excited sound wave travelling back- and forthwards through the Sun interior (Musman 1974). This corresponds roughly to the sound speed:

$$V_{\rm S} \sim \frac{R_\odot}{5\,{\rm min}} \approx 2.3 \times 10^8\,{\rm cm\,s^{-1}}. \tag{5}$$

Roth, Howe & Komm (2002) have suggested that internal flows can have a maximum sectorial amplitude of about $10^3\,{\rm cm\,s^{-1}}$. They argue that a higher velocity would lead to a noticeable distortion of the rotation rate in the convection zone. In this case, the Mach number reads (see Table 2):

$$\mathcal{M} = \frac{V_{\rm HD}}{V_{\rm S}} \sim 10^{-4}. \tag{6}$$

Consequently, the fluid motions in the Sun are compressible with extremely low Mach numbers.

Similarly, in the case of neutron stars, the temperature of the superfluid ranges between 10^7 and 5×10^8 K, depending on the crust heat source (Van Riper 1991). The superfluid velocity relative to coordinates rotating with angular velocity $\Omega_{\rm NS}$ can reach $V_{\rm HD} \approx 10^4$–$10^6\,{\rm cm\,s^{-1}}$ (Jones 2003).

Thus, the ratio of the sound crossing time to the hydrodynamical time-scale reads

$$\frac{\tau_{\rm S}}{\tau_{\rm HD}} \approx \left(\frac{V_{\rm HD}}{V_{\rm S}}\right)^2 = \mathcal{M}^2 \approx 10^{-6}, \tag{7}$$

where $V_{\rm S}^2[={\rm d}P/{\rm d}\rho = (\rho - \frac{1}{3}p)/(\rho + p)]$ corresponds to the sound speed squared, which is roughly 10 per cent of the speed of light, depending on the equation of state.

The flows in these two extreme astrophysical objects indicate that numerical solvers should be robust enough to deal with extremely low Mach number flows. Such flow conditions are encountered when trying to model the origin of the solar dynamo or the thermonuclear ignition of hydrogen rich matter on the surface of neutron stars, considered to be responsible for Type-I X-ray bursts (Fisker et al. 2005) or for novae eruption in the case of white dwarfs (Camenzind 2007).

In this paper, a non-linear Newton-type solver for modelling weakly incompressible flows is presented. The paper is organized as follows. In Section 2, we compare the mathematical formulation of both compressible and extremely incompressible flows. The new numerical solver is presented and discussed in Section 3 while in Section 4 we verify the robustness of this solver by applying it to Taylor–Couette flows between two concentric spheres, followed by a summary in Section 5.

2 COMPRESSIBLE VERSUS WEAKLY AND STRONGLY INCOMPRESSIBLE FLOWS

While the equations describing compressible and incompressible flows are apparently similar, the underlying physics and the corresponding numerical treatments are fundamentally different.

Table 1. Scaling variables for non-dimensioning the hydrodynamical equations.

Scaling	Variables	Neutron star (interior)
$\tilde{L}$	Length	$\sim 10^6$ cm
$\tilde{\rho}$	Density	$\sim 10^{14}\,{\rm g\,cm^{-3}}$
$\tilde{\mathcal{T}}$	Temperature	$\sim 10^7$ K
$\tilde{\mathcal{P}}$	Pressure	$\sim 10^{26}\,{\rm dyn\,cm^{-2}}$
$\tilde{V}$	Velocity	$\sim 10^6\,{\rm cm\,s^{-1}}$
$\tilde{B}$	Magnetic fields	$\sim 10^9$ G
$\tilde{\mathcal{M}}$	Mass	$\sim {\rm M}_\odot$

Table 2. Non-dimensional numbers. In this list, the additional parameters ν, $\nu^{\rm mag}$, $\nu_{\rm T}$ and $\tilde{V}_{\rm g}$ correspond to hydrodynamical viscosity, magnetic diffusivity, heat diffusion coefficient and the effective velocity of the potential energy Ψ (i.e. $\tilde{V}_g^2 = \nabla\tilde{\Psi}$), respectively.

Name	Symbol	Definition
Reynolds number	Re	$\tilde{V}\,\tilde{L}/\nu$
Mach number	$\mathcal{M}$	$\tilde{V}/\tilde{V}_S$
Reynolds number (magnetic)	$\rm Re^{mag}$	$\tilde{V}\,\tilde{L}/\nu^{\rm mag}$
Mach number (magnetic)	$\mathcal{M}^{\rm mag}$	$\tilde{V}_A/\tilde{V}_S$
Prantl number	Pr	$\nu/\nu_{\rm T}$
Froude number	Fr	$(\tilde{V}/\tilde{V}_{\rm g})^2$
Peclet number	Pe	Re · Pr

In general, compressible flows are made of plasmas. The internal macroscopic motions may become either supersonic or extremely sub-sonic. Incompressible flows, however, are generally made of liquid, so that a further compression would not lead to a noticeable change in their density. The transition from the gas phase to the fluid phase mostly does not occur via a smooth change of the equation of state. For example, a high pressure acting on to a container of hot water vapour cannot be asymptotically extended to describe the pressure in a normal water fluid. Therefore, from the astrophysical point of view, weakly incompressible flows can be viewed as strongly compressed plasmas, in which the macroscopic velocities are relatively small compared to the sound velocity.

To clarify these differences, we write the set of hydrodynamical equations in a non-dimensional form using the scaling variables listed in Table 1.

The set of magnetohydrodynamical equations describing compressible plasmas in a conservativeform is as follows.

(i) Continuity equation:

$$\frac{\partial\rho}{\partial t} + \nabla\cdot\rho V = 0. \tag{8}$$

(ii) The momentum equations:

$$\frac{\partial\rho V}{\partial t} + \nabla\cdot(\rho V\otimes V) = -\frac{1}{\mathcal{M}^2}\nabla P + \frac{\rho}{{\rm Fr}^2}\nabla\Psi + \left(\frac{\mathcal{M}_{\rm mag}}{\mathcal{M}}\right)^2 \nabla\times B\times B + \frac{1}{\rm Re}\nabla\cdot\sigma, \tag{9}$$

where $\sigma = \eta(\nabla V + (\nabla V)^{\rm T}) - \frac{2}{3}\eta(\nabla\cdot V)I$, $\eta = \rho\nu$ and $\nabla\Psi$ are the Reynolds stress tensor, the dynamical viscosity and the gradient of the potential energy, respectively.

(iii) The total energy equation:

$$\frac{\partial \mathcal{E}}{\partial t} + \nabla \cdot (\mathcal{E} + p)V = \left(\frac{\mathcal{M}}{\mathrm{Fr}}\right)^2 \rho \nabla \Psi \cdot V + \left(\frac{\mathcal{M}}{\mathrm{Re}}\right)^2 \nabla \cdot (V\sigma) + \frac{1}{\mathrm{Pe}} \nabla \cdot (\nu_{\mathrm{T}} \nabla T), \tag{10}$$

where $\mathcal{E} = \rho(\varepsilon + \frac{1}{2}V^2)$ and ν_{T} is the heat diffusion coefficient. We may simplify the total energy equation by separating the internal energy from the mechanical energy and assuming a perfect conservation of the latter. Hence, we are left with an equation that describes the time evolution of the internal energy:

$$\frac{\partial \mathcal{E}^d}{\partial t} + \nabla \cdot \mathcal{E}^d V = -(\gamma - 1)\mathcal{E}^d \nabla \cdot V + (\gamma - 1)\left\{ \left(\frac{\mathcal{M}}{\mathrm{Re}}\right)^2 \Upsilon + \frac{1}{\mathrm{Pe}} \nabla \cdot (\nu_{\mathrm{T}} \nabla T) \right\}, \tag{11}$$

where Υ ($\doteq \eta\, |\nabla \cdot V|^2$) is the dissipation function.

(iv) Magnetic equation.

The magnetic induction equation, taking into account transport and diffusion in a non-dimensional form, reads

$$\frac{\partial B}{\partial t} = \nabla \times \left\langle V \times B - \frac{1}{\mathrm{Re}^{\mathrm{mag}}} \left(\frac{\mathcal{M}^{\mathrm{mag}}}{\mathcal{M}}\right) \nabla \times B \right\rangle. \tag{12}$$

To close the system of equations, we use the equation of state: $P = P(\rho, T) = (\gamma - 1)\rho\varepsilon$, where γ denotes the adiabatic index and ε the specific internal energy of the flow. In Section 3, we describe a numerical solution procedure for solving the set of the compressible hydrodynamical equations, i.e. equations (8), (9) and (11), in the low Mach number limit and verify its robustness in Section 4.

On the other hand, incompressible flows are described through the following set of equations:

$$\nabla \cdot V = 0 \text{ (This corresponds to constant density)} \tag{13}$$

$$V_t + (V \cdot \nabla)V = -\nabla P + \frac{1}{\mathrm{Fr}^2} \nabla \Psi + \frac{1}{\mathrm{Re}} \nabla \cdot \sigma \tag{14}$$

$$\frac{\partial T}{\partial t} + \nabla \cdot TV = \text{constant } \Upsilon + \frac{1}{\mathrm{Pe}} \nabla \cdot (\nu_{\mathrm{T}} \nabla T). \tag{15}$$

Despite the apparent similarity, the pressure in compressible flows has different physical meanings; in the compressible case the equation of energy influences the momentum equation through the equation of state, whereas in the incompressible case the pressure is just a Lagrangian multiplier with no direct physical meaning.

This implies that equations (14) and (15) cannot be coupled through the classical equation of state corresponding to ideal flows. The set of equations of incompressible flows is characterized by the following two features:

(i) the velocity field must not only evolve as described by the momentum equations, but it should also fulfil the divergence-free condition;

(ii) there is no direct equation that describes the time evolution of the pressure.

Therefore, we may use the pressure in the momentum equations to form an equation that enforces the flow to move in such a manner that the divergence-free condition is always fulfilled, independent of the constitutive nature of the flow.

This can be achieved by taking the divergence of the above momentum equation:

$$\nabla \cdot \left[V_{\mathrm{t}} + (V \cdot \nabla)V - \frac{1}{\mathrm{Fr}^2} \nabla \Psi - \frac{1}{\mathrm{Re}} \nabla \cdot \sigma \right] = -\nabla \cdot \nabla P = -\Delta P, \tag{16}$$

which can be rewritten in the following compact form:

$$\Delta P = \mathrm{RHS}. \tag{17}$$

The right-hand side (RHS) contains the divergence of the other terms of the momentum equations.

We note that the strategy of turning ∇P in the momentum equations into a Poisson like-equation is one of the cornerstones of the projection method suggested by Chorin and Temam for modelling incompressible flows (Rannacher R. 2009, private communication; see Prohl 1997 for further details). This method, however, cannot be used to model highly stratified flows in astrophysics. In the following, we mention a few of these limitations.

(i) The pressure gradient must be a smoothly varying function of space. This condition is also necessary to assure that

$$\nabla \cdot V \sim \frac{\partial}{\partial t} \nabla \cdot V \sim \Delta P \approx 0,$$

which implies that the proposed flow must be weakly compressible.

(ii) In the limit of hydrostatic equilibrium,[1] the following approximation holds:

$$\nabla P \sim \rho g_{\mathrm{eff}},$$

where g_{eff} denotes the effective gravity, i.e. the sum of all forces including the centrifugal one.

Assuming the flow to be isothermal and non-rotating, we obtain, as a solution, the density profile $\rho \sim \mathrm{e}^{-1/r}$. Note that, although $\nabla \cdot V \approx 0$, the expression $\frac{\partial^2}{\partial r^2}\rho$ vanishes nowhere. This implies that using $\Delta P = \mathrm{RHS}$ to determine the pressure would smooth ∇P and fail to maintain the hydrostatic equilibrium.

(iii) Contrary to the internal or total energy equation, the divergence theorem of Gauss cannot be applied to an equation of the form $\Delta P = \mathrm{RHS}$. This theorem is a necessary condition to assure the conservation of physical quantities. Therefore, determining the pressure from the latter equation is not sufficient for assuring the conservation of energy. We note that ∇P is a geometry-dependent quantity and therefore is not invariant under coordinate transformations.

Moreover, as long as the gradient of the pressure does not vanish at the boundaries, the pseudo-pressure resulting from the Poisson operator would violate the global conservation of energy.

It is important to note that compressibility and incompressibility characterize two completely different states of matter. The transition from one phase to another depends on the chemical potential and microscopic properties of the molecules constituting the flow matter. These two states cannot be described by a single and simple equation of state. Pressure terms appearing in the equations describing incompressible flows are rather mathematical terms, usually called Lagrangian multipliers, and which are used to constrain the global motion of the flow with no thermodynamical reasoning.

Some approaches use the splitting method of the pressure into thermodynamical and mathematical parts (see Ratzel 2004, and the

[1] For example, when the density ρ varies with radius and $\rho = \rho(p)$.

© 2009 The Authors. Journal compilation © 2009 RAS, MNRAS **400,** 903–916

references therein). Such strategy is rather ad hoc which requires fine-tuning of the two pressures to meet special requirements of the specific flow problem.

The construction of a Poisson-like operator for the pressure is the basis of different variants of the so-called projection methods, such as the 'Semi-Implicit Method for Pressure-Linked Equation' (SIMPLE) and 'Pressure-Implicit with Splitting Operator' (PISO; see Barton 1998, for further details). Similarly, the projection method can also be applied to the induction equation in magnetohydrodynamics. Here the induction equation (12) is modified to include the gradient of a scalar function Θ as follows:

$$\frac{\partial B}{\partial t} = \nabla \times \langle V \times B + \cdots \rangle + \nabla\Theta. \tag{18}$$

Taking the divergence of this equation, we obtain

$$\nabla \cdot B \approx \delta t \times \Delta\Theta. \tag{19}$$

As before, this method violates the conservation of the magnetic flux. $\nabla\Theta$ appearing in the induction equation is a source function for generating or annihilating the magnetic flux. Such a source term may generate magnetic monopoles from the zero magnetic flux, which is a severe violation of the conservation of the magnetic flux.

To elaborate this point, let $\nabla\Theta =$ constant and let $V = v^{\rm mag} = 0$. In this case, $B(t) = at + b$, where a and b are constants. Thus, although $\Delta\Theta = 0$, the magnetic flux may still grow indefinitely. This implies that a constant pumping of the magnetic flux due to numerical errors cannot be eliminated by applying a Poisson-like operator.

The matrix form of the projection method applied to the momentum equation (14) and to the Poisson equation (17) is as follows:

$$\begin{bmatrix} J & G \\ G^* & 0 \end{bmatrix} \begin{bmatrix} V^{n+1} \\ P^{n+1} \end{bmatrix} = \begin{bmatrix} \mathrm{RHS} \\ 0 \end{bmatrix}, \tag{20}$$

where the coefficient matrices $J = \partial L_{\rm m}/\partial V$, $G = \partial L_{\rm m}/\partial P$, $G^* = \partial L_{\rm p}/\partial V$ and '$n+1$' corresponds to the values at the new time level. $L_{\rm m}$ and $L_{\rm p}$, respectively, denote equations (14) and (17) in an operator form. Applying Lower-Upper triangular matrix decomposition (LU-decomposition), the matrix equation (20) can be rewritten as

$$\begin{bmatrix} J & 0 \\ G^* & -G^*J^{-1}G \end{bmatrix} \begin{bmatrix} I & J^{-1}G \\ 0 & I \end{bmatrix} \begin{bmatrix} V^{n+1} \\ P^{n+1} \end{bmatrix} = \begin{bmatrix} \mathrm{RHS} \\ 0 \end{bmatrix}, \tag{21}$$

where I denotes the identity matrix. This equation is solved in two steps:

$$\begin{aligned} &I. \quad \begin{bmatrix} J & 0 \\ G^* & -G^*J^{-1}G \end{bmatrix} \begin{bmatrix} V^* \\ P^* \end{bmatrix} = \begin{bmatrix} \mathrm{RHS} \\ 0 \end{bmatrix} \\ &II. \quad \begin{bmatrix} I & J^{-1}G \\ 0 & I \end{bmatrix} \begin{bmatrix} V^{n+1} \\ P^{n+1} \end{bmatrix} = \begin{bmatrix} V^* \\ P^* \end{bmatrix}. \end{aligned} \tag{22}$$

In general the inversion of the Jacobian, J, is difficult and costly, and it is therefore suggested to replace it by the pre-conditioning $\tilde{A}$. In this case, the above-mentioned two-step solution procedure should be reformulated and solved using the defect-correction iteration procedure:

$$\begin{aligned} &\text{(I)} \quad \begin{bmatrix} \tilde{A} & 0 \\ G^* & -G^*\tilde{A}^{-1}G \end{bmatrix} \begin{bmatrix} \delta V^* \\ \delta P^* \end{bmatrix} = \begin{bmatrix} d \\ 0 \end{bmatrix} \\ &\text{(II)} \quad \begin{bmatrix} I & \tilde{A}^{-1}G \\ 0 & I \end{bmatrix} \begin{bmatrix} \delta V^{n+1} \\ \delta P^{n+1} \end{bmatrix} = \begin{bmatrix} \delta V^* \\ \delta P^* \end{bmatrix}, \end{aligned} \tag{23}$$

where $\delta P^* = P^* - P^n$, $\delta P^{n+1} = P^{n+1} - P^*$ and $d = \mathrm{RHS} = JV^*$.

Using a different approach that relies on the finite volume strategy applied to compressible low Mach flows, Guillard & Viozat (1998) showed that the discrete equations support pressure fluctuations of the order of $\mathcal{M}$, whereas the continuous equations support pressure fluctuations of the order of $\mathcal{M}^2$. As a consequence, one may split P into a small 'compressible' pressure of the order of $\mathcal{M}^2$ superimposed on to an 'incompressible' background pressure.

Based on such extension, a multiple pressure variable (MPV) method for modelling weakly compressible and shock-free flows has also been suggested by Munz et al. (2003). Following this scenario, it is argued that in the low Mach number regime ($\mathcal{M} \ll 1$), the variables can be expanded in the following manner:

$$q = q^{(0)} + \mathcal{M}\, q^{(1)} + \mathcal{M}^2\, q^{(2)} + \cdots. \tag{24}$$

Under classical conditions, the MPV method requires the leading terms in the expansion of the pressure to be constant in order to assure matching of the solutions in the asymptotic limit. However, in the regimes that interest us, e.g. stellar interiors, the leading terms must vanish or be spatially varying functions in order to establish a hydrostatic equilibrium. In this case, the pressure must decrease non-linearly with radius, so to stably oppose the gravitational force of the central object.

Almgren et al. (2006) studied the time evolution of an injected heat bubble in the atmosphere of a neutron star using different types of numerical approximations aimed at properly treating compressible flows in the low Mach number limit. They find that their suggested low Mach number approximation (LMNA) performs relatively well compared to pure incompressible or inelastic approximations. The strategy relies on finding an appropriate function β_0, which must fulfil the constrain $\nabla \cdot \beta_0 V = \beta_0 \mathcal{F}$, where $\mathcal{F} = \mathcal{F}(P, \rho)$ (see equation 17 in Almgren et al. 2006). We however note that violent fluid motions associated with Type-I X-ray bursts are most likely of a high Mach number type, so that the method of finding the appropriate β may break down.

Lin, Bayliss & Taam (2006) proposed the LMNA method to study X-ray bursts on the surface of a non-rotating neutron star. Their method relies on filtering the sound speed from the hydrodynamical equations, which, in the case of neutron stars, exceeds the fluid motion by at least two orders of magnitude. Thus, the time-step size used here to advance the evolution of the flow can be as large as $\delta t \sim {\rm d}x/V$, where V is the fluid velocity.

Indeed, using this strategy, the authors were able to run hydrodynamical calculations far beyond the sound speed crossing time.

However, as the background state is assumed to be near hydrostatic equilibrium, violent bursts that are governed by strong time-dependent fluid motions, the LMNA method may fail to treat such flow configurations properly.

3 HIGHLY COMPRESSED LOW MACH FLOWS: AN ITERATIVE NON-LINEAR PRE-CONDITIONED NEWTON SOLVER

3.1 Preliminaries

For completeness, we describe in the following several numerical conventions that are useful for understanding the solution procedure described in the next section.

Define the operator of the continuity equation:

$${\rm d}L_\rho = \frac{\partial \rho}{\partial t} + \frac{\partial}{\partial x}\rho U + \frac{\partial}{\partial y}\rho V, \tag{25}$$

where U and V are the velocity components in the x and y directions, respectively.

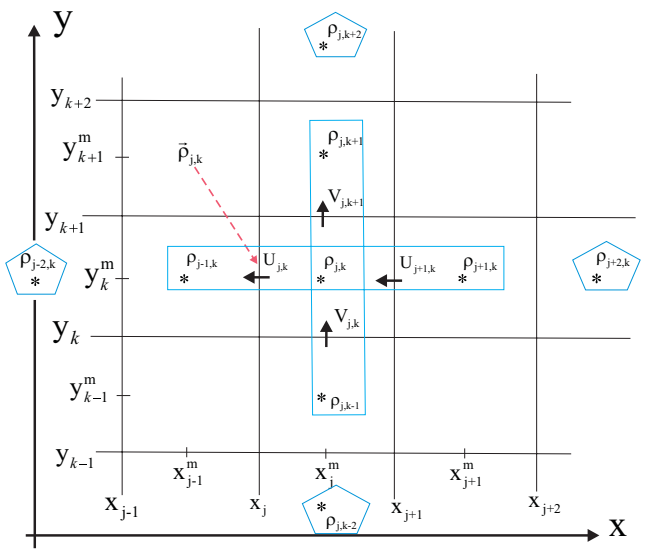

Figure 1. The staggered grid strategy: the localization of the variables in five- and nine-point finite volume discretization. '*j*' and '*k*' are the grid numbering in the *x*- and *y*-directions, respectively.

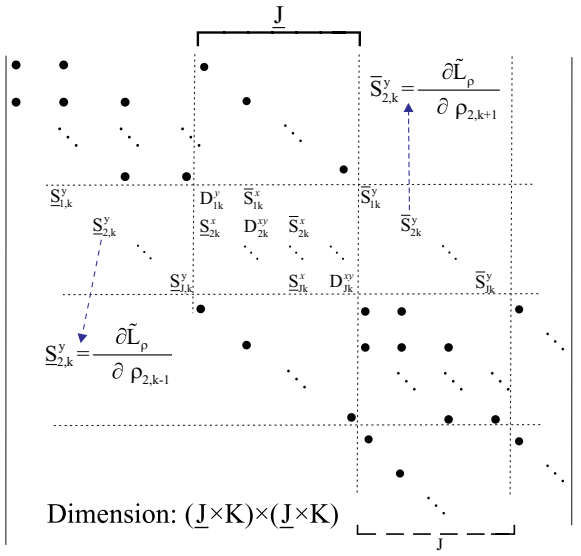

Figure 2. The coefficient matrix with its penta-diagonal entries resulting from implicit formulation of the continuity equation in two dimensions using the staggered-grid discretization. The matrix is of $N \times N$ dimensions, where $N = \underline{J} \times K$ is the total number of grid points; '*J*' and '*K*' are the number of grid points in the *x*- and *y*-directions, respectively.

A consistent finite volume discretization requires defining the material flux at cell surfaces and scalars at their centres (see Fig. 1).

Using finite volume discretization, the operator gets the following discretized form:

$$\delta L_\rho = \left[\frac{\delta\rho_{j,k}}{\delta t}\right] + \left[\frac{U_{j+1,k}\boldsymbol{\rho}_{j+1,k} - U_{j,k}\boldsymbol{\rho}_{j,k}}{\Delta x_j}\right] + \left[\frac{V_{j,k+1}\boldsymbol{\rho}_{j,k+1} - V_{j,k}\boldsymbol{\rho}_{j,k}}{\Delta y_k}\right], \quad (26)$$

where $\delta\rho_{j,k} = \rho^{n+1}_{j,k} - \rho^n_{j,k}$, $\Delta x_j = x_{j+1} - x_j$ and $\Delta y_k = y_{k+1} - y_k$. The superscript '$n$' denotes the last time level and '$n+1$' denotes the next (future) one. $\boldsymbol{\rho}_{j,k}$ stands for the density at the interface of the cell, which can be calculated using low or highly spatially accurate advection schemes (see Section 3.1.1).

We may now define the corresponding 'new' defect:

$$d^{n+1}_\rho = -\left[\frac{\delta\rho_{j,k}}{\delta t}\right] - \left[\frac{U_{j+1,k}\boldsymbol{\rho}_{j+1,k} - U_{j,k}\boldsymbol{\rho}_{j,k}}{\Delta x_j}\right]^{n+1} - \left[\frac{V_{j,k+1}\boldsymbol{\rho}_{j,k+1} - V_{j,k}\boldsymbol{\rho}_{j,k}}{\Delta y_k}\right]^{n+1}, \quad (27)$$

and the 'old' defect:

$$d^n_\rho = -\left[\frac{\delta\rho_{j,k}}{\delta t}\right] + \left[\frac{U_{j+1,k}\boldsymbol{\rho}_{j+1,k} - U_{j,k}\boldsymbol{\rho}_{j,k}}{\Delta x_j}\right]^{n} + \left[\frac{V_{j,k+1}\boldsymbol{\rho}_{j,k+1} - V_{j,k}\boldsymbol{\rho}_{j,k}}{\Delta y_k}\right]^{n}, \quad (28)$$

Using the damped Crank–Nicolson method (Hujeirat & Rannacher 2001), we may combine these two expressions to form a temporary second-order accurate scheme:

$$\delta L_\rho = \vartheta d^{n+1}_\rho + (1-\vartheta) d^n_\rho, \quad (29)$$

where $\vartheta = \frac{1}{2} + \frac{\delta t}{1+\delta t}$ is the Crank–Nicolson parameter and δt is set to be less than unity for accuracy reasons.

The left-hand side (LHS) of this equation can be viewed as a variational displacement which can be expanded as a function of the variable ρ to form a defect-correction procedure:

$$\delta L_\rho = \frac{\partial L_\rho}{\partial \rho}\delta\rho = J\delta\rho, \quad (30)$$

where J is the corresponding Jacobian (see e.g. Fig. 2).

Thus, equation (29) gets the following matrix form:

$$J\delta\rho = \vartheta d^{n+1}_\rho + (1-\vartheta) d^n_\rho. \quad (31)$$

3.1.1 *Spatial accuracy*

The values of $\boldsymbol{\rho}_{j,k}$ across the cell surfaces in equations (27) and (28) are calculated using the Monotone Upstream-Centered Schemes for Conservation Laws or simply the MUSCL schemes (see Hirsch 1988, and the references therein). MUSCL is most suitable for implicit solvers, as their construction does not depend on the time-step size explicitly. A general MUSCL-type scheme in one dimension gives the following interface values:

$$\boldsymbol{\rho}_{j,k} = \begin{cases} \rho_j - \frac{1}{4}[(1+\kappa)\Delta\rho_j + (1-\kappa)\Delta\rho_{j+1}] & \text{if } V_j \le 0 \\ \rho_{j-1} + \frac{1}{4}[(1-\kappa)\Delta\rho_j + (1+\kappa)\Delta\rho_{j-1}] & \text{if } V_j > 0, \end{cases} \quad (32)$$

where $\Delta\rho_j = \rho_j - \rho_{j-1}$, κ is a switch off/on parameter used to specify the accuracy needed. Second-order spatial accuracy corresponds to $\kappa = 1$ whereas $\kappa = 1/3$ corresponds to third-order accuracy.

3.1.2 *The construction of the pre-conditioning*

In constructing the pre-conditioning $\tilde{A}$, we reformulate δL_ρ using a low-resolution advection scheme, specifically the first-order upwind scheme:

$$\boldsymbol{\rho}_{j,k} = \begin{cases} \rho_{j,k} & \text{if } V_j \le 0 \\ \rho_{j-1,k} & \text{if } V_j > 0. \end{cases} \quad (33)$$

We note that the low order accuracy is useful in order to assure a stable inversion procedure of $\tilde{A}$ and minimize the corresponding computational costs. In this case, the LHS of equation (29) may be

expanded as follows:

$$\delta\tilde{L}_\rho = \frac{\partial \tilde{L}_\rho}{\partial \rho^{n+1}}\,\delta\rho = \left[\vartheta\,\frac{\partial \tilde{d}_\rho^{n+1}}{\partial \rho^{n+1}}\right]\delta\rho = \tilde{A}\delta\rho, \tag{34}$$

where $\tilde{d}_\rho^{n+1}$ is the defect calculated using a low-resolution and numerically diffusive advection scheme.

The final form of the defect-correction iteration procedure reads

$$\tilde{A}\delta\rho = \vartheta d_\rho^{n+1} + (1-\vartheta)d_\rho^n. \tag{35}$$

Note that while the LHS of this equation is calculated using a low-resolution scheme, the RHS is evaluated using the best possible resolution. These different evaluation strategies requires performing additional iterations in each time-step to assure mathematical consistency.

At an arbitrary grid point (j,k), this equation has the form

$$\begin{array}{lll} & \overline{S}^y_{j,k}\delta\rho_{j,k+1} & \\ + \underline{S}^x_{j,k}\delta\rho_{j-1,k} & + D^{x,y}_{j,k}\delta\rho_{j,k} & + \overline{S}^x_{j,k}\delta\rho_{j+1,k} = d_\rho^{\rm mod}, \\ & + \underline{S}^y_{j,k}\delta\rho_{j,k-1} & \end{array} \tag{36}$$

where $d_\rho^{\rm mod} = \vartheta\ d_\rho^{n+1} + (1-\vartheta)d^n{}_\rho$ and where

$$\begin{aligned} \underline{S}^x &= \frac{\partial \tilde{L}_\rho}{\partial \rho^{n+1}_{j-1,k}}, \quad \overline{S}^x = \frac{\partial \tilde{L}_\rho}{\partial \rho^{n+1}_{j+1,k}} \\ \underline{S}^y &= \frac{\partial \tilde{L}_\rho}{\partial \rho^{n+1}_{j,k-1}}, \quad \overline{S}^y = \frac{\partial \tilde{L}_\rho}{\partial \rho^{n+1}_{j,k+1}} \\ D^{x,y} &= \frac{\partial \tilde{L}_\rho}{\partial \rho^{n+1}_{j,k}}. \end{aligned} \tag{37}$$

The location of these entries in the approximate Jacobian $\tilde{A}$ is shown in Fig. 2, where the under- and over-lines assign the sub- and super-diagonal entries, respectively.

3.1.3 *Partial updating of the pressure in low Mach number flows*

The momentum equations describing low Mach number non-magnetized flows may be rewritten as

$$\frac{1}{\mathcal{M}^2}\nabla P = \text{RHS}, \tag{38}$$

where the RHS consists of the remaining parts of equation (9). In the absence of external forces, such as gravity, stationarity implies that RHS $\sim \mathcal{M}^2 \ll 1$ and that, although the pressure is large, its spatial variation must be relatively small.

In this case, we may take the divergence of the equation to obtain

$$\triangle P = \mathcal{M}^2\nabla\cdot\text{RHS}. \tag{39}$$

Using a uniform grid distribution and applying finite volume discretization, the discretized form of this equation at an arbitrary grid point (j,k) reads

$$\begin{array}{lll} & P_{j,k+1} & \\ + P_{j-1,k} & -4P_{j,k} & + P_{j+1,k} = \mathcal{M}^2\nabla\cdot\text{RHS}, \\ & + P_{j,k-1} & \end{array} \tag{40}$$

and whose corresponding Jacobian is shown in Fig. 3. Since P is relatively large compared to the RHS and since the sum of pressure terms altogether is small, a solution procedure that relies on updating just a part of the pressure terms most likely would fail to converge. To clarify this point we note that the ADI solution method relies on solving only three of six pressure terms implicitly, whilst the other

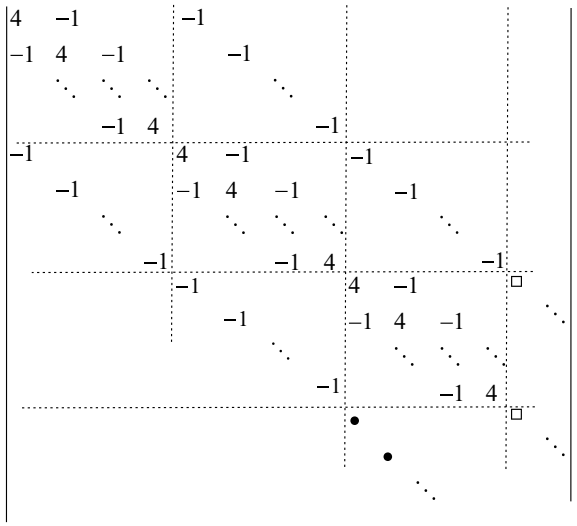

Figure 3. The real Jacobian resulting from finite volume discretization of the Poisson equation of the pressure. Except for the AFM, pre-conditionings that rely on partial updating of the pressure terms are found to diverge.

remaining three terms are computed 'almost' explicitly, as shown in the following two-step procedure:

$$\begin{aligned} &(1)\ P^*_{j-1,k} - 2P^*_{j,k} + P^*_{j+1,k} = -P^n_{j,k-1} + 2P^n_{j,k} - P^n_{j,k+1} \\ &\qquad\qquad + \mathcal{M}^2\nabla\cdot\text{RHS}, \\ &(2)\ P^{n+1}_{j,k-1} - 2P^{n+1}_{j,k} + P^{n+1}_{j,k+1} = -P^*_{j-1,k} + 2P^*_{j,k} - P^*_{j+1,k}, \end{aligned}$$

where the P values on the RHS are assumed to be known, whereas those on the LHS are the sought unknowns.

Similarly, the line-Gauss–Seidel (LGS) method also relies on solving four terms implicitly while the other two terms are recovered through repeated directional sweepings:

$$\begin{aligned} &(1)\ P^*_{j-1,k} - 4P^*_{j,k} + P^*_{j+1,k} = -P^i_{j,k-1} - P^i_{j,k+1}, \\ &\qquad\qquad + \mathcal{M}^2\nabla\cdot\text{RHS}, \\ &(2)\ P^{n+1}_{j,k-1} - 4P^{n+1}_{j,k} + P^{n+1}_{j,k+1} = -P^*_{j-1,k} - P^*_{j+1,k}. \end{aligned}$$

The numerical errors generated through decomposing the pressure terms into different classes that are treated with different numerical solution procedures may significantly slow the convergence of the global solution procedure.

Extending this analysis into a set of four equations that describe the time evolution of the variables $\boldsymbol{q} = (\rho, U, V, P)$, a penta-block matrix of the form displayed in Fig. 5 would result.

Using a highly accurate advection scheme in constructing the pre-conditioning would lead to a significant enlargement of the bandwidth of the pre-conditioning (see Fig. 4), hence increasing the computational costs considerably.

If we were to use a second-order accurate advection scheme in constructing the pre-conditioning, then the bandwidth of the one-dimensional part, i.e. the sub-diagonal $\underline{S}^x$, the super-diagonals $\bar{S}^x$ and the diagonal block matrices D^{xy} shown in Fig. 5, would increase from[2] $3 \times 4 \times N$ to $5 \times 4 \times N$. As the algebraic manipulation required for inverting a matrix of bandwidth 'm' scales as

[2] 3 = number of blocks, 4 = number of equations and N = number of grid points.

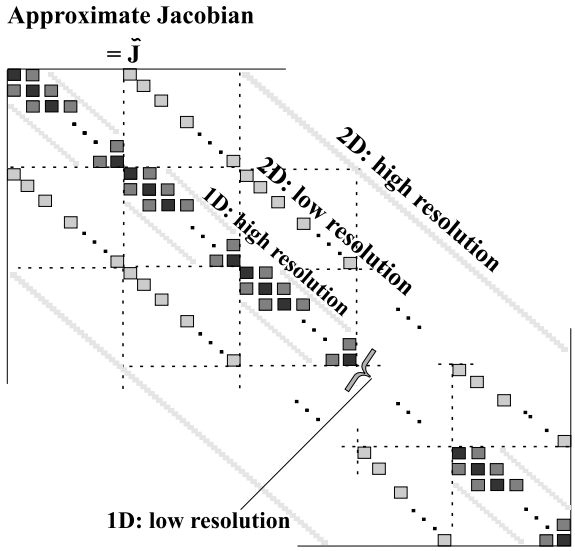

Figure 4. The approximate Jacobian matrix $\tilde{J}$, in which entries corresponding to low and high spatial resolutions in one and two dimensions are taken into account. The dashed lines show quadratic sub-matrices corresponding to the variable along the x-axis: from $j = 1$ to $j = J$ and constant k.

m^2 times the number of grid points, the inclusion of entries corresponding to second-order accuracy raises the computational costs by 250 per cent. In the multidimensional case, however, solving the non-ordered set of the Navier–Stokes equations while using a spatially accurate advection scheme would yield a Jacobian of the form displayed in Fig. 6, whose direct inversion is difficult and computationally prohibitive.

3.2 The global solution procedure

Assume we are given a two-dimensional non-linear vector equation of the form

$$\frac{\partial q}{\partial t} + \frac{\partial F(q)}{\partial x} + \frac{\partial G(q)}{\partial y} = f, \tag{41}$$

where q, F, G, f denote the vector of variables, their momentum flux in both x- and y-directions and a source function, respectively.

Define the residual $d(q)$ and look for the vector q, such that $d(q) = 0$, i.e.

$$d(q) = f - \left[\frac{\partial q}{\partial t} + \frac{\partial F(q)}{\partial x} + \frac{\partial G(q)}{\partial y}\right] = 0. \tag{42}$$

The non-linear Newton finite difference formulation of this residual reads

$$d(q^{\mathrm{i+1}}) = f^{\mathrm{i+1}} - \left[\frac{q^{\mathrm{i+1}} - q^{\mathrm{n}}}{\delta t} + \frac{\Delta_x F(q^{\mathrm{i+1}})}{\Delta x} + \frac{\Delta_y G(q^{\mathrm{i+1}})}{\Delta y}\right] = 0,$$

where 'i' denotes the iteration number. Having numerically obtained $d(q^{i+1}) = 0$, we can then set q^{i+1} to be equal to 'q' at the new time level '$n + 1$'. In the case of a single one-dimensional non-linear function $\mathcal{F}(x) = 0$, the zeros can be found using the Newton iteration method:

$$x^{i+1} = x^i - \frac{\mathcal{F}}{\dot{\mathcal{F}}}, \tag{43}$$

where $\dot{\mathcal{F}}(x^i) = \frac{\partial \mathcal{F}}{\partial x}|_{x=x^i}$. When applying this approach to a general system of equations such as equation (41), we then have to perform

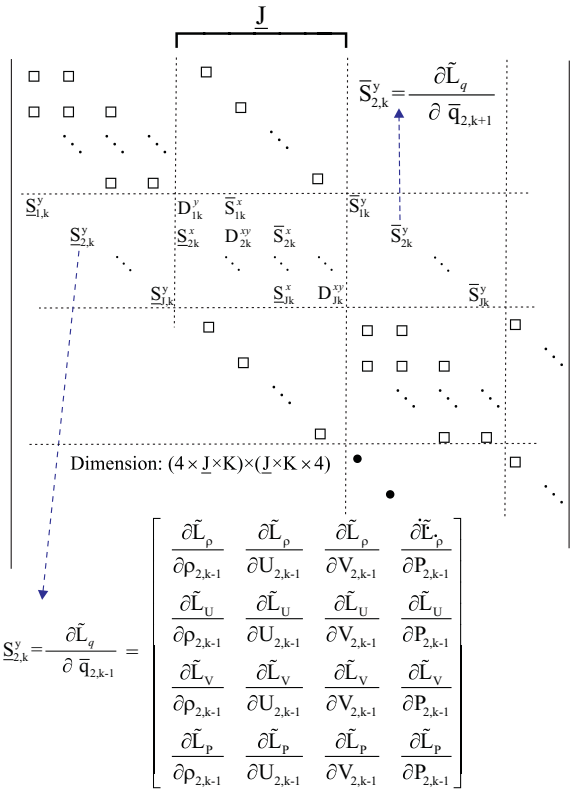

Figure 5. The coefficient matrix with its penta-block diagonal entries resulting from implicit formulation of four equations consisting of the continuity, two momentum and energy equations in two -dimensions using the staggered-grid discretization.

the following replacements:

$$\left.\begin{array}{c} x \mapsto q \\ \mathcal{F}(x) \mapsto d(q) \\ \dot{\mathcal{F}} \mapsto J \end{array}\right\} \Rightarrow q^{i+1} = q^i - J^{-1} d\,, \tag{44}$$

where J is the real Jacobian matrix defined as $J = \frac{\partial d}{\partial q}$ (see Figs 4 and 6). Defining $\mu = q^{i+1} - q^i$, we may rewrite equation (44) as

$$J\,\mu = d, \tag{45}$$

where 'd' is calculated using arbitrary high spatial and temporal accuracies.

The matrix equation (45) is said to be

$$\begin{cases} \text{Linear :} & \text{if } d = d(q^n) \\ \text{Otherwise :} & \text{if } d = d(q^i), \end{cases} \tag{46}$$

where 'n' corresponds to the old time level and 'i' to the iteration level. While in the first case, one needs to invert the Jacobian once per time-step, in the second case, however, several iterations per time-step might be required to recover the non-linearity of the solution. The calculation may become prohibitively expensive, if the Jacobian to be inverted corresponds to a system of equations in multidimensions to be solved with high spatial and temporal accuracies.

The idea of pre-conditioning is to calculate the defect 'd' as proposed by the physical problem (e.g. with very high resolution), whereas the real Jacobian J is then replaced by an approximate matrix $\tilde{A}$ of the following properties:[3]

[3] We equivalently denote the approximate Jacobian as $\tilde{A}$ or $\tilde{J}$.

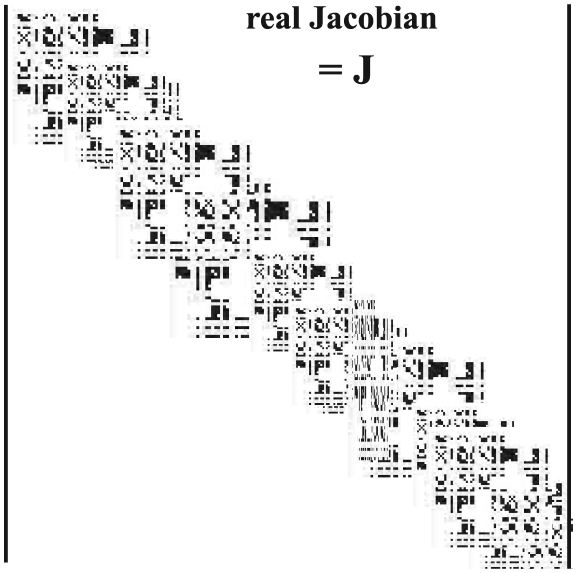

Figure 6. A schematic picture of a Jacobian, J, that possibly results from finite volume discretization of the Navier–Stokes equation in 2D. J is a highly sparse matrix with a lot of zero entries.

(i) $\tilde{A}$ is easier to invert than J,
(ii) $\tilde{A}$ and J are similar and share the same spectral properties.

While the first property is easy to fulfil, the second one is in general an effort-demanding issue. It states that the pre-conditioning $\tilde{A}$ should differ only slightly from the Jacobian if trivial replacements are to be avoided. Therefore, given the matrix $\tilde{A}$, the solution procedure would run as follows.

(i) Compute the defect 'd'.
(ii) Use the matrix equation $\tilde{A}\,\mu = d$ to solve μ.
(iii) Update $q^{i+1} = q^i + \mu$ and recalculate 'd' and $\tilde{A}$, respectively.
(iv) Procedures (ii) and (iii) should be repeated until max ($|d|$) is smaller than a number ϵ, where the maximum runs over all the elements of 'd'.

The fundamental question to be addressed still is: how to construct a robust pre-conditioner $\tilde{A}$ that is capable of modelling low Mach number flows efficiently, but still easy to invert? In this construction, two essential constraints should be taken into account as follows.

(i) A conservative first-order spatial discretization of the Navier–Stokes equations generally yields a Jacobian matrix of a penta-diagonal block form as depicted in Fig. 5.
(ii) The gradients of the thermal pressure are dominant, so that all pressure-connected terms must be treated simultaneously.

In order to clarify these two points, we rewrite the matrix equation (45) at an arbitrary grid point (j,k) in the following block form:

$$\begin{array}{lll} & \overline{S}^{y}_{j,k}\mu_{j,k+1} & \\ + \underline{S}^{x}_{j,k}\mu_{j-1,k} & + D^{\rm mod}_{j,k}\mu_{j,k} & + \overline{S}^{x}_{j,k}\mu_{j+1,k} = d_{j,k} \\ & + \underline{S}^{y}_{j,k}\mu_{j,k-1}, & \end{array} \tag{47}$$

where $\underline{S}^{x,y}$ and $\overline{S}^{x,y}$ denote the sub- and super-diagonal block matrices and $D^{\rm mod} = I/\delta t + D^x + D^y$ the diagonal block matrices, respectively.

While this block structure is best suited for using the one-coloured or multicoloured LGS iterative method, test calculations have shown, however, that these iterative methods may stagnate or may even diverge if the flow is of a low Mach number type. The reason for this behaviour is that most iterative methods rely either on partial updating of the variables or on the dimensional splitting. These, however, are considered to be inefficient methods or they may even stagnate, if the corresponding system of equations to be solved is of an elliptic type, such as the Poisson equations.

One way of considering the different multidimensional variations of the pressure all at one time is to spatial-factorize the Jacobian into sub-matrices, such that the resulting multiplication results in a good approximation of the original Jacobian, i.e.

$$J \mapsto \Pi_{lm}\tilde{A}_l\tilde{A}_m, \tag{48}$$

where $\tilde{A}_i$ is a coefficient matrix consisting of entries that correspond to the operators in the i dimension. Such a splitting depends, of course, on the discretization method used and, in particular, on the manner the gradient of pressure is treated in the discrete space. For example, the sub-matrix $\tilde{A}_i$ should necessarily contain the coefficients of $\partial P/\partial x_i$ in the respective direction.

The advantage of this procedure is that the dimensions of the scheme can be gradually increased; hence, it is easy to verify its consistency and accuracy. Furthermore, the RHS, i.e. the defect, is updated only after the inversion of the matrices $\tilde{A}_i$ is complete. We note that this pre-conditioner can be used even as a direct solver as long as time-dependent solutions are concerned. To clarify this procedure, we simplify equation (41) and write it in the finite space as follows:

$$\frac{\delta q}{\delta t} + \frac{\Delta_x F^{n+1}}{\Delta x} + \frac{\Delta_y G^{n+1}}{\Delta y} = 0, \tag{49}$$

where $\delta q = q^{n+1} - q^n$ (μ) and $\Delta_{x,y}$ are space difference operators. Force terms have been omitted for clarity.

We may expand F^{n+1} and G^{n+1} around their values at the old time levels as follows:

$$\begin{aligned} F^{n+1} &= F^n + \delta t \left(\frac{\partial F}{\partial t}\right)^n + \mathcal{O}(\delta t)^2 \\ &= F^n + \delta t \left(\frac{\partial F}{\partial q}\right)^n \left(\frac{\partial q}{\partial t}\right)^n + \mathcal{O}(\delta t)^2 \\ &\mapsto F^n + \delta t A^n \left(\frac{\delta q}{\delta t}\right)^n + \mathcal{O}(\delta t)^2. \end{aligned}$$

Equivalently,

$$F^{n+1} = F^n + A^n\delta q + \mathcal{O}(\delta t)^2,$$

$$G^{n+1} = G^n + B^n\delta q + \mathcal{O}(\delta t)^2. \tag{50}$$

Substituting these expressions into equation (49), we obtain

$$\left[\frac{I}{\delta t} + L_xA^n + L_yB^n + \mathcal{O}(\delta t)^2\right]\delta q = L_xF^n + L_yG^n, \tag{51}$$

where L_x and L_y denote the differential operators in the x- and y-directions, respectively. We may replace equation (51) by the following approximation:

$$\left[\frac{I}{\delta t} + L_xA^n\right]\left[I + \delta t\, L_yB^n\right]\delta q = L_xF^n + L_yG^n. \tag{52}$$

This replacement induces an error which is proportional to $\delta t\, L_x\, L_y + \mathcal{O}(\delta t)^2$. This error may diminish for steady conserved fluxes, but may diverge for time-dependent solutions if the time-steps are large. The latter disadvantage is relaxed by the physical consistency requirement that small time-steps are to be used if the

sought solutions are time dependent. The matrix equation (51) can be rewritten in the following compact form:

$$\tilde{A}_x \, \tilde{A}_y \mu = d, \tag{53}$$

where $\tilde{A}_x = \frac{I}{\delta t} + L_x A^n$ and $\tilde{A}_y = I + \delta t \, L_y B^n$. Comparing equations (45) and (53), it can be easily verified that

(i) the RHS of both equations is identical;

(ii) the Jacobian 'J' on the LHS of equation (45) is replaced by $\tilde{A}_x \, \tilde{A}_y$ on the LHS of equation (53);

(iii) similar to 'J', ∇P is fully incorporated in $\tilde{A}_x$ and in $\tilde{A}_y$. This means that the coefficients $\partial L_{\boldsymbol{m}} / \partial P_{[(j-1,j,j+1),k]}$ and $\partial L_{\boldsymbol{m}} / \partial P_{[j,(k-1,k,k+1)]}$ are fully taken into account in building up the sub-block $\bar{S}^x$, $\bar{S}^y$, $\underline{S}^x$, $\underline{S}^y$ and $D^{x,y}$ (see Fig. 5). $L_{\boldsymbol{m}}$ denotes the momentum equations in an operator form.

We note that item (i) is a vital requirement here, as it implies that after performing a sufficient number of iterations, the resulting numerical solution of both equations must be identical.

Item (ii) implies that if equation (45) were to be solved directly, then the corresponding computational costs would scale as $I_1 \times N^3$, where $N \times N$ is the dimension of the Jacobian and I_1 the number of global iterations required to recover the non-linearity of the equations per time-step. These costs are by far much more higher than $2 \times I_2 \times m^2 \times N$ required for completely solving equation (53), where 'm' is the bandwidth of the matrix $\tilde{A}_x$ and I_2 is the number of global iterations required for recovering the non-linearity of the equations.

The third item is crucial too, as ∇P or equivalently the low Mach number properties of the flow essentially determine the properties of the matrix $\tilde{A}$ to be inverted, in particular its condition number. In the case of extremely small low Mach number flows, e.g. $\mathcal{M} < 10^{-3}$, the pressure-related coefficients are the dominant entries in the off-diagonal block matrices $\underline{S}^{x,y}$ and $\overline{S}^{x,y}$ (see equation 47). In this case, the pre-conditioner $\tilde{A}$ may easily become ill-conditioned and its inversion may become unstable. As a consequence, although the solution procedure presented here performs well for high and moderately low Mach number flows, it is not suited for searching stationary flow configurations in which $\mathcal{M} \gg 10^{-3}$.

Applying this factorization within a non-linear iterative solution procedure, the iterative solution procedure would run as follows.

(i) Compute the defect $d = d(q^i, q^n)$ at each grid point using the best available spatial and temporal accuracies.

(ii) Solve the matrix equation $\tilde{A}_y \delta q^* = d$, to obtain δq^*.

(iii) Solve the matrix equation $\tilde{A}_x \delta q = \delta q^*$ to obtain δq.

(iv) Update q: $q^{i+1} = q^i + \delta q$ and subsequently the defect d.

(v) Perform a convergence check to verify if max $(|d|) < \epsilon$. If not, then the above-mentioned algorithmic steps should re-iterated.

We note that procedures (ii) and (iii) are interchangeable without affecting the convergence of the solution procedure or the accuracy of the resulting solutions. The role of pre-conditioning in this procedure can be elaborated as follows.

(i) Let $Jq = b$ be the matrix equation to be solved, where 'b' is the vector of known quantities and J is the exact Jacobian corresponding to the set of hydrodynamical equations.

(ii) The defect 'd' is computed using the best available temporal and spatial discretization methods (see e.g. Section 3.1.1). According to equation (44), this is equivalent to computing the defect from $d = b - Jq^i$.

(iii) The approximate Jacobian, i.e. the pre-conditioner $\tilde{A}$, is used to solve the corrector μ from the matrix equation $\tilde{A}\mu = d$.

(iv) We then use the obtained corrector μ to calculate the vector of unknowns on the new iteration level as follows:

$$q^{i+1} = q^i + \mu.$$

But this is equivalent to

$$q^{i+1} = q^i + \tilde{A}^{-1} d = q^i + \tilde{A}^{-1}(b - Jq^i).$$

Consequently, obtaining $\mu = 0$ after a certain number of iterations implies that $q^{i+1} = q^i$, which means that $Jq^i = b$. Thus, q^i is a solution for the linear system $Jq = b$, in which the coefficient matrix is the exact Jacobian J. Note that once the exact solution q^i is recovered, the final solution does not depend on the nature of the pre-conditioner, which implies consistency of the numerical procedure with the original hydrodynamical equations as well as in accord with the classical pre-conditioning philosophy for solving linear systems of equations (Turkel 1993).

The pre-conditioning presented here act mainly on the spatial part of the equations. For example, the off-diagonal block matrices that correspond to higher spatial resolution (see Fig. 4) are neglected when constructing the pre-conditioner $\tilde{A}$, but are fully taken into account in the differential operators of 'd'. The block matrices corresponding to higher dimensions are included in the construction of the pre-conditioner, as described in equation (48).

This pre-conditioning techniques enable handling dominant pressure gradients in the low Mach number regime without violating or modifying the compressibility of the hydrodynamical equations. It is valid and applicable for both shock-free and shock-dominated flows (i.e. discontinuous pressure) with or without viscosity.

This procedure differs conceptually from the compressible-SIMPLE methods worked out by Karki & Patankar (1989) and Munz et al. (2003). Here one still needs to solve a Poisson equation for correcting the pressure, provided the pressure is continuous and sufficiently smooth, which therefore applies only to a very limited class of astrophysical flows.

We note that other robust pre-conditioning methods for accelerating the convergence of both incompressible and compressible hydrodynamical equations have been suggested by Turkel (1993) and Turkel & Vatsa (2005). These pre-conditionings act on the time derivatives of the variables; hence, their effect disappears when the steady-state solutions are recovered. Similar pre-conditioning techniques have also been employed by Guillard & Viozat (1998) for modelling compressible Euler-type flows in the low Mach number limit.

3.3 Generalization: multidimensions and general EOS

Extending equation (41) into 3D, the vector equation then reads

$$\frac{\partial q}{\partial t} + \frac{\partial F(q)}{\partial x} + \frac{\partial G(q)}{\partial y} + \frac{\partial H(q)}{\partial z} = f, \tag{54}$$

where H denotes the momentum flux in the z-direction.

Similar to equation (50), we may linear-expand H^{n+1} to obtain an equivalent form to equation (51) in 3D:

$$\left[\frac{I}{\delta t} + L_x A^n + L_y B^n + L_z C^n + \mathcal{O}(\delta t)^2\right] \delta q$$

$$= L_x F^n + L_y G^n + L_z H^n, \tag{55}$$

where C^n is the matrix resulting from the linear expansion of H^{n+1}.

© 2009 The Authors. Journal compilation © 2009 RAS, MNRAS **400,** 903–916

The LHS of this equation can be approximated by the following matrix multiplication:

$$\mathrm{LHS} \mapsto \left[\frac{I}{\delta t} + L_x A^n\right]\left[I + \delta t\, L_y B^n\right]\left[I + \delta t\, L_z C^n\right]$$

$$\doteq \tilde{A}_x\, \tilde{A}_y \tilde{A}_z, \tag{56}$$

and to finally obtain the defect-correction iteration procedure in 3D:

$$\tilde{A}_x\, \tilde{A}_y \tilde{A}_z \delta q = d, \tag{57}$$

where the 3D defect is defined as

$$d(q^{i+1}) = f^{i+1} - \left[\frac{q^{i+1} - q^n}{\delta t} + \frac{\Delta_x F(q^{i+1})}{\Delta x} + \frac{\Delta_y G(q^{i+1})}{\Delta y} + \frac{\Delta_y H(q^{i+1})}{\Delta z}\right].$$

Similar to equation (31), the spatial and temporal accuracies of the defect can be accordingly modified.

A possible pre-conditioned defect-correction iterative solution procedure could run as follows.

(i) Solve $\tilde{A}_x \mu^* = d, \mapsto \mu^*$.
(ii) Solve $\tilde{A}_y \mu^{**} = \mu^*, \mapsto \mu^{**}$.
(iii) Solve $\tilde{A}_z \delta q = \mu^{**}, \mapsto \delta q \mapsto q^{n+1} = q^n + \delta q$.

We note that the implementation of the AFM-pre-conditioning techniques is not restricted to a certain class of equations of state. It should be stressed here that what determines the consistency of the mathematical equations in the finite space with the original physical problem is the defect in the first place, whereas the role of a pre-conditioning is generally to speed up convergence and enhance the stability of the numerical solution procedure. Thus, one may use even the identity matrix as a pre-conditioning in combination with the Jacobi iteration (Hujeirat 2005). Although the method may converge, it generally requires an unacceptably large number of iterations per time-step. Thus, if the pressure appears in the equations as a primary variable, then the coefficients resulting from $\partial L^H_{\boldsymbol{m}}/\partial P$ are computable and their incorporation in the pre-conditioning is then a straightforward procedure.

On the other hand, if the coefficient $\partial L^H_{\boldsymbol{m}}/\partial P$ is not available directly, then we may expand this derivative in the form $(\partial L^H_{\boldsymbol{m}}/\partial E)(\partial E/\partial P))$, where $E = E(q,\, P)$ is a primary variable. This expression can then be replaced by an adequate approximation. The suitability of this approximation is then measured through the number of additional iterations per time-step required for keeping the defect sufficiently small.

4 ROTATING LOW MACH NUMBER FLOWS BETWEEN TWO CONCENTRIC SPHERES

4.1 Taylor flows between two concentric spheres

Large-scale motions of gas in stellar spherical shells are controlled by the imbalance of energies, namely among the potential, thermal, rotational and magnetic energies. It is generally accepted that rotation deforms surfaces of constant pressure, but has only indirect influence on surfaces of constant temperatures. The resulting baroclinicity is unbalanced and derives large-scale meridional circulation (Sweet 1950). On the local scale, these flows are in general convectively unstable; hence, they are governed by convective turbulence. Such combined motions are observationally evident in the solar convective zone.

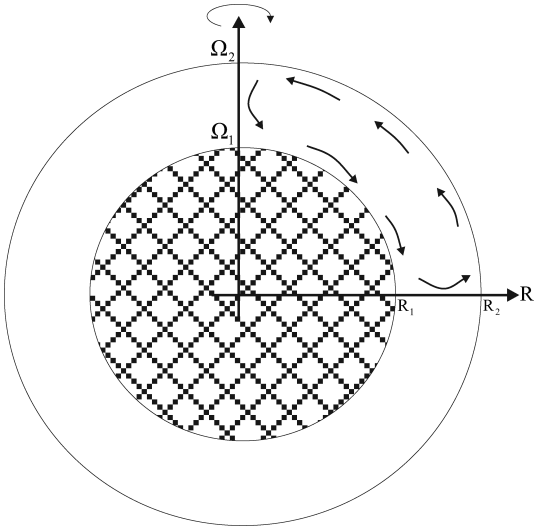

Figure 7. Two concentric spheres: the inner sphere has a radius R_1 and rotates with angular velocity Ω_1 whereas the outer one has the radius R_2 and rotates with Ω_2.

In the laboratory, spherical Couette flows between two rotating spheres are considered to be similar to rotating stellar envelopes. In the case of fast rotation, the flow is a combination of primary azimuthal rotations and a secondary meridional circulation induced by Ekman pumping (Greenspan 1968). Here the flow is controlled by two parameters: the Reynolds number and the gap width between the two spheres. The Reynolds number for this configuration is defined as

$$\mathrm{Re} = \frac{|\Delta\Omega| R_1 |\Delta R|}{\nu} = \frac{|\Omega_2 - \Omega_1| R_1 |R_2 - R_1|}{\nu}, \tag{58}$$

where $R_{1,2}$, $\Omega_{1,2}$ and ν are the inner and outer radii, the angular frequency of the inner and outer sphere and viscosity, respectively (Fig. 7).

The number of rotationally induced fluid vortices and transition to turbulence in Couette flows depend on how large the Reynolds number is as well as on the width δ of the gap between the two spheres. For example, for $\mathrm{Re} > 460$ and $\delta = \frac{R_2 - R_1}{R_1} = 0.006$ Couette flows have been verified to become turbulent (Gertsenshtein et al. 2001).

In applying our solver to Couette flows between two concentric spheres, the set of compressible hydrodynamical equations in conservative finite volume formulation is solved. The set of equations solved here consists of equations (8), (9) and (11), where we assume $\nabla\Psi = \boldsymbol{B} = 0$ and $\Upsilon = \nu_T = 0$. We use the equation of state (EOS) of an ideal gas with $\gamma = 5/3$. For viscosity, the following α-viscosity prescription for modelling small-scale turbulence is used:

$$\nu_{\mathrm{tur}} \doteq \langle V_{\mathrm{tur}}\rangle \langle \ell_{\mathrm{tur}}\rangle \approx \alpha_{\mathrm{tur}} V_{\mathrm{S}} \times \alpha_2 R_{\mathrm{NS}}, \tag{59}$$

where $\langle\, V_{\mathrm{tur}}\rangle$ and $\langle \ell_{tur}\rangle$ correspond to the mean values of velocity and length-scales of eddies in the turbulent medium, respectively. $\langle V_{\mathrm{tur}}\rangle$ is set to be smaller than the sound speed, V_{S}, and the length-scale $\langle \ell_{\mathrm{tur}}\rangle$ is set to be a small portion of the radius of the inner sphere. Thus, α_{tur} and α_2 are constants that are smaller than unity. In this paper, all model calculations assume $\langle \ell_{\mathrm{tur}}\rangle = 0.1 R_{\mathrm{in}}$, i.e. $\alpha_2 = 0.1$, whereas the parameter α_{tur} may differ from one model calculation to another.

In addition, the following parameters have been used: $\Omega_{\mathrm{in}} = 3$, $\Omega_{\mathrm{out}} = 0$, $R_{\mathrm{in}} = 1$, $R_{\mathrm{out}} = 1.25$ and a viscosity coefficient $\alpha_{\mathrm{turb}} = 0.005$ (see Fig. 8). The distributions of the density and temperature

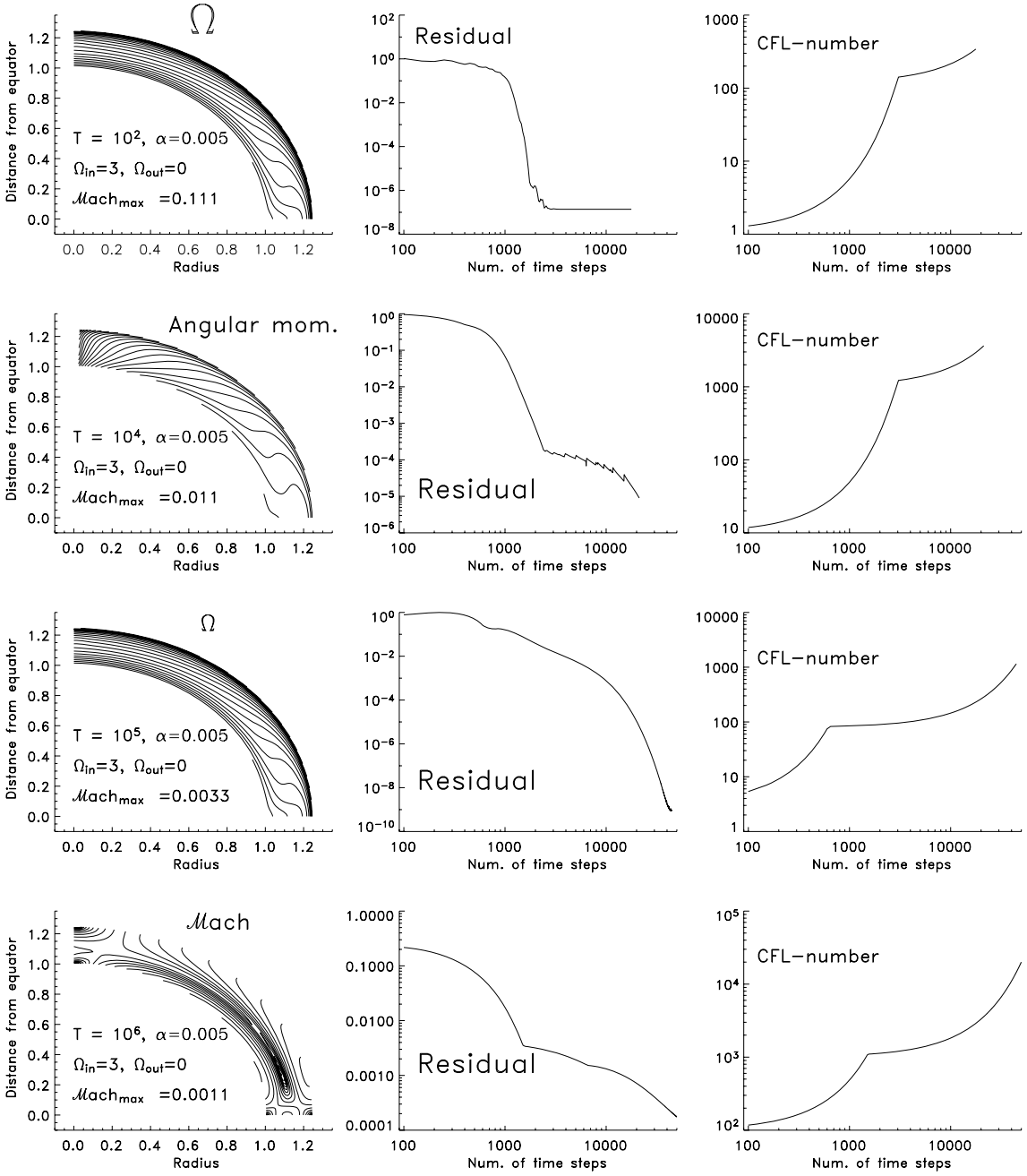

Figure 8. Taylor–Couette flows: the inner sphere has a radius $R_{\rm in} = 1$ and rotates with $\Omega_{\rm in} = 3$, whereas the outer sphere has a radius $R_{\rm out} = 1.2$ and $\Omega_{\rm out} = 0$. The flow has the constant viscosity coefficient $\alpha = 0.005$. The Mach number is set to decrease systematically by increasing the initial temperature from $T = 10^2$ up to $T = 10^6$ in separate runs. This corresponds to a reduction of the Mach number by two orders of magnitude. In the middle panel, the development of the residual versus the number of time-steps in each separate run is shown. The right-hand panel shows the corresponding time evolution of the time-step size in units of the Courant number.

are set to be initially uniform. All runs are initiated using the same uniform density $\rho(r, \theta, t = 0) = 1$, but using different initial uniform temperatures: $T(r, \theta, t = 0) = 10^2$ for Run1, $T(r, \theta, t = 0) = 10^4$ for Run2, $T(r, \theta, t = 0) = 10^5$ for Run3 and $T(r, \theta, t = 0) = 10^6$ for Run4, where ρ, T are given in the units listed in Table 1.

The domain of calculation is limited to the first quadrant $[1 \leq R \leq 1.25] \times [0 \leq \theta \leq \pi/2]$. Along the equator and polar axis reflecting boundary conditions have been imposed, whereas a zero material flux across the outer and inner boundaries has been used. We use a temporally first-order but spatially third-order MUSCL-type scheme for finite modelling the advection terms in the defect, whereas first-order upwinding is used in constructing the preconditioner. The domain of calculations has been sub-divided into 50 uniform finite volume cells in the radial and 120 in the polar directions, respectively.

In order to test the capability of the solver to deal with low Mach number flows, we have run several calculations using different initial values of the temperature ranging from 10 up to one million. This corresponds to a reduction of the Mach number by three orders of magnitude.

We have carried out several test calculations using different types of pre-conditionings that are based on LGS iterative procedures as well as on the AFM (see equation 53).

Using a moderate CFL number,[4] i.e. CFL ≈ 10, we found that pre-conditioners that are based on partial updating of the pressure, such as LGS methods, ADI or operator splitting, diverge quickly with decreasing $\mathcal{M}$. On the other hand, using the AFM as a pre-conditioner in combination with a defect-correction Newton iteration procedure is capable of modelling weakly compressible flows down to $\mathcal{M} \approx 10^{-3}$ (see Fig. 4.) The Ω distributions shown in Fig. 8 are stationary solutions, that have been obtained after the maximum residual of the angular momentum equation has dropped below a certain value ϵ_Ω. The time-step size in these calculations is set to increase with decreasing residual.

Although the final flow configurations obtained in all runs are stationary, the history of the residuals is found to differ from one run to another. We attribute this behaviour to the simple but still-to-be improved time-step control, which presently relies on a time extrapolation procedure to compute the 'future' time-step size and which is found to be rather sensitive to the Mach number, especially when it becomes small. To clarify this point, we mention that the weight of the pressure terms in equation (9) increases quadratically with a decreasing Mach number. Their corresponding coefficients contribute to the off-diagonal entries of $\tilde{A}$ and scale as $\mathcal{M}^{-2}$. In the case of extremely low Mach number flows, the positive contribution to the diagonal is due to the term $\delta\rho V/\delta t$, which pre-dominates those of advection and viscous terms. In this case, the condition number of the matrix, hence the stability of its inversion, is determined mainly by the term $\delta\rho V/\delta t$ and in particular by the size of the time-step. Thus, in the case that stationary solutions are sought, a highly accurate procedure for determining δt is required in order to avoid the generation of artificial perturbations that would unnecessarily slow convergence.

In designing a sophisticated time-step control procedure, previous as well as future values of the maximum residuals evaluated from the whole set of equations should be taken into account.

4.2 Rotating highly stratified flows in the deep interior of relativistic objects

The model problem adopted here is rotating flows in the shell of an ultra-compact neutron star (UCNS). The domain of calculation is taken to be the first quadrant:

$$\mathcal{D} = [R_{\rm in} \le r \le R_{\rm out}] \times [0 \le \theta \le \pi/2]$$
$$= [1 \le r \le 1.5] \times [0 \le \theta \le \pi/2],$$

where length-scales are measured in units of the radius of the UCNS.

We assume that UCNS reside inside their last stable orbits. The radius of the UCNS is calculated using the expression

$$R_{\rm NS} = 3\, r_g\, (1 + \sqrt{1 - \Omega_{\rm NS}^2}), \qquad (60)$$

where $r_g = GM_{\rm NS}/c^2$, G is the gravitational constant, $M_{\rm NS} = 1.44\,{\rm M}_\odot$ and 'c' is the speed of light. Note that the radius of the UCNS can be smaller than the classical last stable orbit of a Schwarzschild black hole. The inner boundary of the domain of calculation is taken to be $R_{\rm NS}$, whereas the outer boundary is located at $R_{\rm out} = 1.5 R_{\rm NS}$. The UCNS is set to rotate rigidly with $\Omega_{\rm NS}$, which is taken to be 33 per cent of the break-up velocity whereas the outer sphere is set to rotate with zero angular velocity ($\Omega_{\rm out} = 0$.)

Similar to the previous model, the same set of hydrodynamical equations is solved. These equations have been modified to include effects of general relativity, such as the frame-dragging effect of space-time around fast rotating relativistic objects (Hujeirat 1995). We note that the Lorentz factor[5] enhances the coupling and therefore the non-linearities of the hydrodynamical equations (HD) equations in their general relativistic formulation. This has the consequence that a larger number of iterations per time-step would be required to recover the non-linearities of both the defect 'd' and the entries of the pre-conditioner to assure convergence of the non-linear Newton solution procedure compared to the non-relativistic case. Nevertheless, we expect these effects to be small, as most rotating neutron stars rotate at very sub-relativistic speeds.

We use 50 and 120 finite volume cells in the radial and vertical directions, respectively. Logarithmic grid spacing has been used and set to increase from the inner boundary outwards and from the equator upwards. An advection scheme that is spatially of third-order and temporarily of first-order accurate has been used. In obtaining these results, the time-step size is set to increase systematically from the initial value $\delta t = \delta t_{\rm exp}$, which corresponds to CFL $= 1$ up to several hundreds.

Using the units of Table 1, the calculations are initiated with a constant density and temperature and a vanishing velocity field. We use the ideal EOS with $\gamma = 1$. The solver is then applied to search for quasi-stationary hydrodynamical solutions, taking into account the gravitational force of the UCNS as well as the effects of viscosity. Two limiting cases have been considered: a case in which the equations are solved in the Newtonian regime and the case in which general relativistic effects are taken into account. In the latter case, the set of general relativistic Navier–Stokes equations, using the Boyer–Lindquist coordinates in the background of a slowly rotating neutron star (see Hujeirat, Camenzind & Keil 2008, for a detailed derivation of the equations), has been solved.

In Fig. 9, the quasi-stationary 2D distributions of the density, temperature, angular velocity and velocity field in the Newtonian regime (left-hand column) are shown. In the middle column, these distributions are reproduced, taking into account the general relativistic effects. In the latter case, the frame dragging effect resulting from rotating space-time around relativistic objects is expected to leave some imprints on the configurations of rotating flows in deep gravitational fields. In the first three figures of the right-hand column, we over-plotted the radial distributions of the density, angular velocity and temperature along the equator (01 and 11) and along the polar axis (02 and 12). The profiles assigned with 01 and 02 correspond to Newtonian calculations, whereas 11 and 12 to general relativistic calculations.

It is noteworthy that in the general relativistic calculations the poloidal and toroidal components of the velocity are smaller, but the density at the inner radius is larger than those in the Newtonian case (see the radial profiles in the right-hand column of Fig. 9). It should be however noted that the angular velocity plotted here is just that of matter and not the total angular velocity, which includes the velocity of the dragged space in the toroidal direction.

The quasi-stationarity of the solution can be attributed to the formation of vortices near the outer boundary, which appear to change orientation on the viscous time-scale. Also, the non-linearities of

[4] The Courant–Friedrichs–Lewy number is defined as CFL $= (\delta t/\Delta x)/[|V| + V_{\rm S} + (\nu/\Delta x)]$. Thus, CFL ≈ 10 means that acoustic waves are allowed to move across 10 grid points within a single time-step (see Hujeirat 2005a, for further details).

[5] $\Gamma = 1/\sqrt{1-\beta^2}$, where $\beta = V/c$.

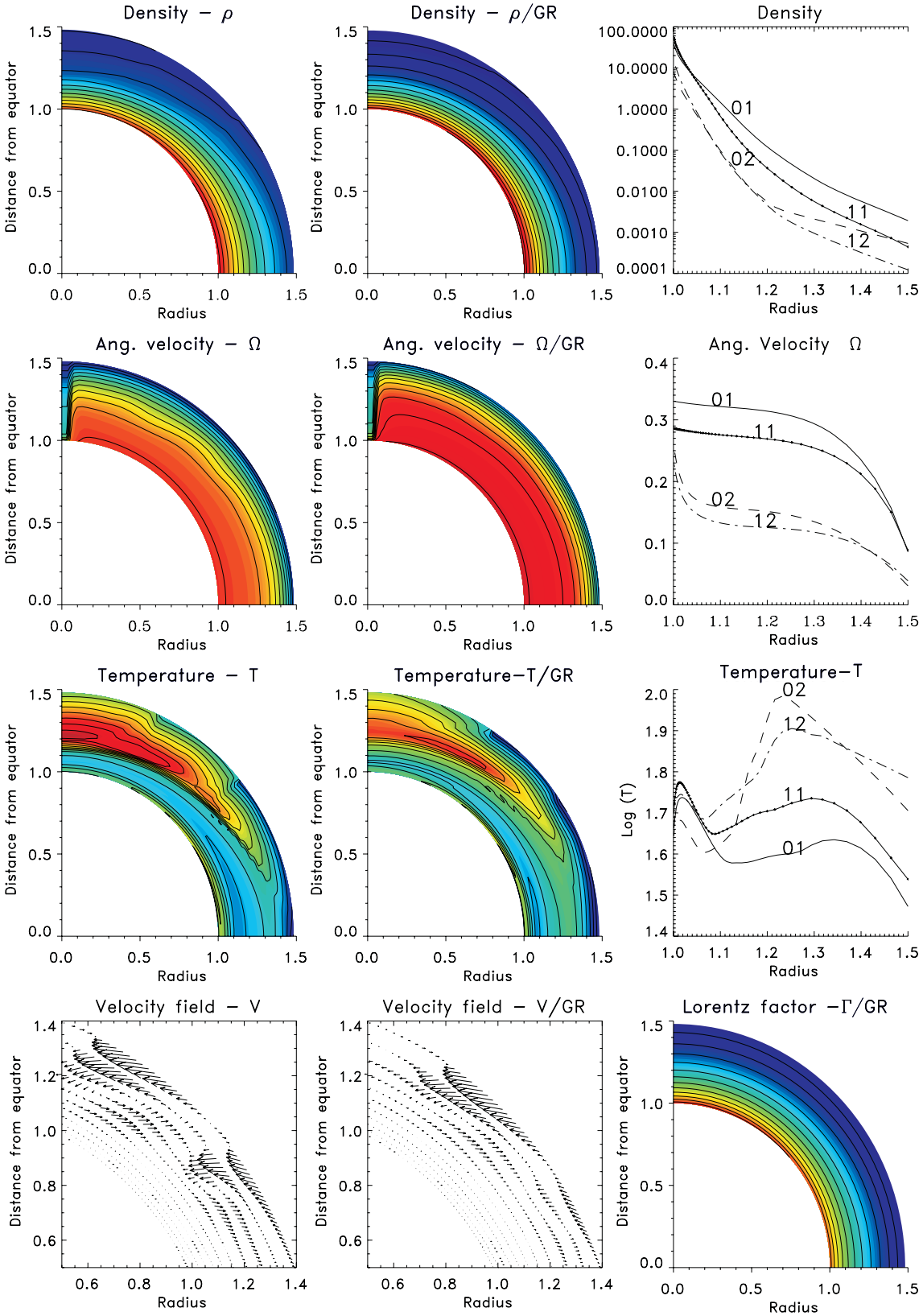

Figure 9. Quasi-stationary rotating flows in a shell of a UCNS. The figures shown in the left-hand column (from top to bottom: density ρ, angular velocity Ω, temperature T and velocity field) correspond to non-relativistic calculations, whereas the images in the middle column (assigned with GR) correspond to general relativistic calculations, including also the distribution of the Lorentz factor in the bottom-right-hand panel. In the right-hand column, we show over-plots of ρ, Ω and T profiles corresponding to both Newtonian and general relativistic calculations. The profiles assigned with '01' and '02' correspond to non-relativistic quantities along the equator and along the polar axis, respectively. '11' and '12' correspond, respectively, to general relativistic quantities along the equator and along the polar axis.

© 2009 The Authors. Journal compilation © 2009 RAS, MNRAS **400,** 903–916

the equations enhanced by strong gravitational fields may hinder the establishment of pure stationary flow configurations.

The calculations here show that our solver, in combination with the AFM as a pre-conditioner, is capable of treating low Mach (in the present case $\mathcal{M} \sim 0.01$) highly stratified and rotating flows under strong Newtonian and general relativistic gravitational fields.

5 SUMMARY

In this paper, we have addressed the numerical difficulties associated with the modelling of rotating and highly stratified flows in the interior of stars and presented a possible solution scenario.

We have shown that stratified rotating flows in the deep interior of normal and compact stars are highly stratified low Mach number flows in which the pressure plays a vital role in dictating their motions and their dynamical stability.

This has the consequence that time explicit methods turn out to be not suited for modelling such flows, as the sound speed crossing time is extremely short relative to the hydrodynamical time-scale. Moreover, classical dimensional splitting of the pressure may destabilize the solution procedure and hinder its convergence.

On the other hand, projection methods that are based on Poisson-like solvers for the pressure would violate the conservative character of the hydrodynamical equations. Determining the pressure from a Poisson-like equation, rather than from the internal or total energy equation, would smooth pressure gradients and hinder the establishment of hydrostatic equilibrium in the interior of stars. This is a consequence of the fact that ∇P is geometry dependent and cannot be treated as an invariant quantity under coordinate transformations.

We have shown that the set of hydrodynamical equations describing the time evolution of rotating, viscous and stratified low Mach number flows is optimally treated using a Newton-type implicit solver in combination with a pre-conditioned defect-correction iteration procedure.

The AFM as a pre-conditioner is shown to be best suited for treating such flows, due to the symmetry preserving character of this method, especially when modelling flows with an isotropic pressure. Unlike the classical non-direct methods that rely on dimensional splitting and/or partial updating, e.g. ADI and LGS, the AFM is based on factorizing the Jacobian matrix and subsequently updating the variable in all directions simultaneously.

We also showed that the AFM-pre-conditioning techniques in principle can be extended into three dimensions, using an arbitrary equation of state.

Finally, we have presented results of several numerical calculations that verify the robustness of the here-presented solution method and its capability to search for quasi-stationary flow configurations under strong gravitational field conditions, both in the Newtonian and in the general relativistic regimes.

We note that the pre-conditioning techniques used here require the inversion of a band matrix of width $m = 12$ in each direction. Therefore, the computational costs in 2D scale as $2 \times N \times m^2$, where N is the number of grid points. This implies that our method is $2 \times 12^2 \approx 300$ slower than their explicit counterparts. On the other hand, it can be easily verified from Fig. 8 that explicit methods must perform approximately 10 000 time-steps (CFL ≤ 1) for every implicit time-iteration (CFL $\sim$ 10 000), in order to capture the here-shown stationary solutions on the same physical time. Consequently, in spite of the fact that our method is 300 times slower, it is still 300 times faster than explicit methods in providing the stationary flow configurations presented here. This estimation is still too optimistic, as most explicit methods work with CFL $\ll 1$. This implies that the time-step size is too small to enable damping the small and unwanted numerical noise, thereby hindering their convergence to complete time-independent flow configurations.

Additionally, implicit methods can also be used for investigating time-dependent and complex flows with sophisticated physical processes that may operate both on much shorter or on much longer time-scales than the hydrodynamical one (see Hujeirat 2005b; Hujeirat et al. 2008; Hujeirat & Heitsch 2009; Hujeirat & Thielemann 2009 for further details).

ACKNOWLEDGMENTS

The authors thank Bernhard Keil for carefully reading the manuscript and Isabelle Baraffe for the fruitful discussion and valuable suggestions during the stay of AH at the Ecole Normale Superieure Centere Astronomique in Lyon. This work is supported by the Klaus-Tschira Stiftung under the project number 00.099.2006.

REFERENCES

Almgren A. S., Bell J. B., Rendleman C. A., Zingale M., 2006, ApJ, 649, 927
Barton I. E., 1998, Int. J. Numer. Methods Fluids, 26, 459
Camenzind M., 2007, Compact Objects in Astrophysics: White Dwarfs, Neutron Stars, and Black Holes. Springer-Verlag, Berlin
Fisker J. L., Brown E., Liebendrfer M., Thielemann F.-K., Wiescher M., 2005, Nuclear Phys. A, 758, 447
Gertsenshtein S. Ya., Zhilenko D. Yu., Krivonosova O. E., 2001, J. Fluid Dynamics, 36, 217
Greenspan H. P., 1968, in Greenspan H., ed., The Theory of Rotating Fluids. Cambridge Univ. Press, Cambridge
Hirsch C., 1988, Numerical computation of internal and external flows. Wiley, New York
Hujeirat A., 1995, JA&A, 295, 268
Hujeirat A., 2005a, J. New Astron., 10, 173
Hujeirat A., 2005b, Comput. Phys. Communications, 168, 1
Hujeirat A., Heitsch F., 2009, Structure Formation in Astrophysics. Cambridge Univ. Press, Cambridge, p. 110
Hujeirat A., Rannacher R., 2001, J. New Astron. Rev., 45, 425
Hujeirat A., Thielemann F.-K., 2009, A&A, 496, 609
Hujeirat A., Camenzind M., Keil B. W., 2008, J. New Astron., 13, 436
Guillard H., Viozat C., 1998, Technical Report 3160. INRIA, Paris, p. 1
Jones P. B., 2003, MNRAS, 340, 247
Karki K. C., Patankar S. V., 1989, AIAA J., 27, 1167
Lin D. J., Bayliss A., Taam R. E., 2006, ApJ, 653, 545
Munz C.-D., Roller S., Klein R., Geratz K. J., 2003, Comput. Fluids, 32, 173
Musman S., 1974, J. Solar Phys., 36, 313
Prohl A., 1997, Advances in Numerical Mathematics. John Wiley & Sons, Chichester
Ratzel M., 2004, PhD thesis, Univ. Stutgart
Roth M., Howe R., Komm R., 2002, JA&A, 396, 243
Sweet P. A., 1950, MNRAS, 110, 548
Turkel E., 1993, Applied Numer. Math., 12, 257
Turkel E., Vasta V. N., 2005, ESIAM: Math. Modelling Numer. Analysis, 39, 515
Van Riper K. A., 1991, ApJ, 372, 251

This paper has been typeset from a TEX/LATEX file prepared by the author.